AD-A209 653

IE CORD

DOCUMENTATION PAGE

Form Approved
OMB No. 0704-0188

1a. REPORT SECURITY CLASSIFICATION UNCLASSIFIED		1b. RESTRICTIVE MARKINGS			
2a. SECURITY CLASSIFICATION AUTHORITY		3. DISTRIBUTION/AVAILABILITY OF REPORT Approved for public release; distribution unlimited			
2b. DECLASSIFICATION/DOWNGRADING SCHEDULE					
4. PERFORMING ORGANIZATION REPORT NUMBER(S)		5. MONITORING ORGANIZATION REPORT NUMBER(S) AFOSR-TR. 89-0787			
6a. NAME OF PERFORMING ORGANIZATION Research Laboratory of Electronics Massachusetts Institute of Technology	6b. OFFICE SYMBOL (If applicable)	7a. NAME OF MONITORING ORGANIZATION AFOSR			
6c. ADDRESS (City, State, and ZIP Code) 77 Massachusetts Avenue Cambridge, MA 02139		7b. ADDRESS (City, State, and ZIP Code) Building 410 Bolling AFB DC 20332-6448			
8a. NAME OF FUNDING/SPONSORING ORGANIZATION United States Air Force	8b. OFFICE SYMBOL (If applicable) NP	9. PROCUREMENT INSTRUMENT IDENTIFICATION NUMBER AFOSR 84-0026			
8c. ADDRESS (City, State, and ZIP Code) Department of the Air Force Air Force Office of Scientific Research Bolling Air Force Base, DC 20332		10. SOURCE OF FUNDING NUMBERS			
		PROGRAM ELEMENT NO. 61102F	PROJECT NO. 2301/	TASK NO. A8	WORK UNIT ACCESSION NO.

11. TITLE (Include Security Classification)

Microwave Emission from Relativistic Electron Beams

12. PERSONAL AUTHOR(S) George Bekefi

13a. TYPE OF REPORT Final	13b. TIME COVERED FROM 11/1/83 TO 10/31/88	14. DATE OF REPORT (Year, Month, Day) March 1989	15. PAGE COUNT 35

16. SUPPLEMENTARY NOTATION

17. COSATI CODES			18. SUBJECT TERMS (Continue on reverse if necessary and identify by block number)
FIELD	GROUP	SUB-GROUP	

19. ABSTRACT (Continue on reverse if necessary and identify by block number)

Profile modification by optical guiding in a Raman free electron laser operating at microwave frequencies was studied experimentally. A cyclotron autoresonance maser (CARM) amplifier was designed, built, and tested. This CARM operates at 35 GHz with a power output of 10 MW and an efficiency of three percent.

DTIC
ELECTE
JUN 2 9 1989
S E D

89 6 29 083

20. DISTRIBUTION/AVAILABILITY OF ABSTRACT ☒ UNCLASSIFIED/UNLIMITED ☒ SAME AS RPT. ☐ DTIC USERS	21. ABSTRACT SECURITY CLASSIFICATION UNCLASSIFIED	
22a. NAME OF RESPONSIBLE INDIVIDUAL Dr Robert J. Barker	22b. TELEPHONE (Include Area Code) 202/767-5011	22c. OFFICE SYMBOL NP

DD Form 1473, JUN 86   Previous editions are obsolete.   SECURITY CLASSIFICATION OF THIS PAGE

UNCLASSIFIED

Final Scientific Report on Grant AFOSR-84-0026

AFOSR·TR· 89-0787

for research on

Microwave Emission from Relativistic Electron Beams

for the period

1 November 1987 - 31 October 1988

Submitted by George Bekefi

March 14, 1989

Massachusetts Institute of Technology
Research Laboratory of Electronics
Cambridge, Mass. 02139

Table of Contents

Below is a summary of the work carried out from November 1, 1987 to October 31, 1988.

1. Optical Guiding in Free Electron Lasers

Optical guiding is crucial for the operation of short wavelength free-electron lasers. It mitigates the effects of diffraction and thereby allows the free electron wigglers to exceed the Rayleigh range. We have studied experimentally profile modification of a Raman free electron laser operating at microwave frequencies. Initial studies published in Physical Review Letters are continuing. The final report on this work is given in Appendix 1.

2. The 35 GHz Cyclotron Autoresonance Amplifier

We have had unprecedented success in designing, building, and testing a cyclotron autoresonance maser amplifier. This system operates at a frequency of 35 GHz, with a power output of 10 MW and and an efficiency of 3%. Although CARM oscillators have been built previously in the Soviet Union, we believe that our amplifier is the first of its kind.

A summary of our findings to date is given in Appendix 2. We expect that this work will continue another 12 to 18 months.

Appendix 1

OBSERVATIONS OF FIELD PROFILE MODIFICATIONS
IN A RAMAN FREE ELECTRON LASER AMPLIFIER

K. Xu†, G. Bekefi, and C. Leibovitch‡

Department of Physics and Research Laboratory of Electronics

Massachusetts Institute of Technology

Cambridge, Massachusetts 02139

ABSTRACT

We report measurements of the spatial distribution of the RF electric field intensities and phases induced in a free electron laser (FEL) amplifier operating in the collective (Raman) regime. The studies are carried out at a microwave frequency of ~10 GHz in a FEL using a mildly relativistic electron beam of ~200 keV energy and 1 - 4 A current. The probing of the ponderomotive (space charge) and the electromagnetic waves is accomplished by means of small movable electric dipole antennas inserted into the interaction region.

† permanent address: University of Electronic Science and Technology of China, Chengdu, China.

‡ permanent address: Applied Physics Department, Scientific Division, Rafael Laboratory, Haifa 31021, Israel.

1. INTRODUCTION

Free electron laser (FEL) amplification is the consequence of a resonant interaction [1] between an incident electromagnetic wave and a co-propagating electron beam that has been injected into a periodic "wiggler" magnetic field. This can lead to high output gain, and high efficiency of converting electron beam kinetic energy into radiation. Remarkably, it also leads to large phase shifts [2]-[4] in the amplified electromagnetic wave. Under proper circumstances this phase shift can have a sign such that the electromagnetic wave is refracted towards the axis of the electron beam in a manner somewhat akin to the guiding properties of an optical fiber. Such "optical guiding" [5]-[10] would mitigate the effects of diffraction, and thereby allow the length of FEL wigglers to exceed the Rayleigh range. Long wigglers are needed if free-electron lasers are to operate either in the vacuum-ultraviolet or at high efficiencies in the infrared wavelength regime.

It comes as no surprise that strong FEL activity as described above should be accompanied by significant modification of the spatial distribution of the RF fields within and in the immediate vicinity of the electron beam. To be sure, one way of confirming optical guiding is by observation of the changes in the transverse spatial profile of the copropagating amplified wave. Such field probing can be quite difficult at short wavelengths (infrared and visible). However, the microwave regime, in which our experiments are conducted, offers a relatively simple and direct way. We allow small, movable electric dipole antennas to traverse the waveguide in which the interaction takes place. Using antennas sensitive to different polarizations, we are then able to distinguish between wave types.

There are two major wave types in the vicinity of the bunched electron beam to which our electric dipoles respond. First, there are the electromagnetic (solenoidal) fields associated with the growing electromagnetic wave of frequency ω and axial wavenumber $k_\parallel$, propagating with a velocity $v_p = (\omega/k_\parallel) \geq c$. And then there are the irrotational, quasi-electrostatic fields of the bunched electron beam propagating with a phase velocity $\omega/(k_\parallel + k_w)$ approximately equal to the electron beam velocity $v_b < c$ ($k_w = 2\pi/l_w$ is the wiggler wave number). In the case of tenuous, highly relativistic beams used in short wavelength FELs, the contribution of the space charge electric field to the overall field

profile is usually very small. However, in the microwave regime where often high current, mildly relativistic beams are employed, the contribution from the space charge electric field may no longer be negligible, as will be demonstrated in the experiments described below.

In section 2 of this paper we describe the experimental arrangement. In section 3 we present field profile measurements (in amplitude and phase) associated with the space charge wave. In section 4 we give profiles associated primarily (but not entirely) with the electromagnetic wave. The observations will be discussed in section 5.

2. EXPERIMENTAL SET UP

Figure 1 shows a schematic of our experiment. The accelerating potential is supplied by a Marx generator (Physics International Pulserad 615MR) which has a maximum capability of 500kV and 4kA. Since this accelerator does not use a pulse-forming network, the output voltage pulse is essentially that of a discharging capacitor bank with a shunt adjusted RC time constant of $10 - 100\mu sec$. The electron beam is generated by a thermionically emitting, electrostatically focused, Pierce-type electron gun (250 kV, 250 A) from a SLAC klystron (model 343). An assembly of focusing coils transports the electron beam into the drift tube. To insure good electron orbits, an aperture acting as an emittance selector is inserted which limits the electron beam radius to $r_b = 0.245$ cm so that only the inner portion of the beam is used. With this precaution, the energy spread of the beam entering the magnetic wiggler is $\Delta\gamma_\| / \gamma_\| \leq 0.003$ ($\gamma_\| = [1 - v_\|^2/c^2]^{-\frac{1}{2}}$).

The gun focusing coils guide the electron beam into a rectangular (1.01 cm ×2.29 cm) stainless steel evacuated drift tube which is also the waveguide for the electromagnetic radiation. The beam is contained by an uniform axial magnetic field $B_\|$ that has a power supply limited maximum of 7 kG and a minimum of approximately 800 G. Below this value, beam defocusing and deterioration occur. The net beam current entering the magnetic wiggler is in the range of 1-5 A. The 65 period wiggler magnet has a period $l_w = 3.5$ cm, a maximum amplitude $B_w = 1.0$ kG, and is generated by bifilar conductors. Since the beam aperture limits the size of the beam to $r_b/l_w \approx 0.07$, the wiggler field is close to that of an ideal wiggler. That is, the effects of the radial variation of the wiggler field

3

and the presence of the off-axis components are usually small. At the wiggler entrance a slowly increasing field amplitude is produced by resistively loading the first six periods of the wiggler magnet [11].

The 2.7 m long drift tube acts as a rectangular waveguide whose fundamental TE_{10} mode has a cutoff frequency of $\omega_c/2\pi = 6.6$ GHz. Microwaves are launched onto the electron beam by a waveguide coupler (see Fig. 1). All our measurements are carried out at frequencies between 9 and 11 GHz. At these frequencies the empty waveguide can support only the fundamental (TE_{10}) mode, all higher modes being evanescent. The monochromatic radiation injected into the system is provided by a low power variable frequency source and amplified by means of a traveling wave tube amplifier. Typical power inputs into the FEL are in the 1 - 10 W range. At the output end of the wiggler, a mica window transmits the linearly polarized radiation generated in the drift tube, where it is measured by means of standard calibrated crystal detectors.

The transverse profile of the RF fields is studied by means of three small electric dipole antennas inserted into the waveguide as is illustrated in Figs. 1(b), (c). Two of the antennas, inserted through stainless steel bellows, are movable along the x axis, and their positions are precision controlled by micrometer screws. The third, reference antenna is fixed and protrudes slightly into the waveguide wall as is seen in Figs. 1(b), (c). Each probe has a length of 0.1 cm; cold tests show that the probes can detect RF intensity variations as small as 1% over distances of $\simeq 0.05$ cm. The signal from each probe is attenuated by a variable attenuator, then measured by a calibrated crystal detector. The outputs from the crystal rectifiers are then displayed on fast oscilloscopes. We note that all three antennas are roughly in the middle of the wiggler region and in exactly the same transverse plane, $z \approx 115$ cm from the upstream end of the wiggler.

The left hand movable antenna designated in Figs. 1(b), (c) by $I_y(EM)$ probes the y component of the RF electric field intensity, as does the reference probe $I_y(REF)$. Cold test carried out in the absence of the FEL interaction show that the $I_y(EM)$ probe accurately maps out the TE_{10} waveguide mode whose electric field amplitude is shown schematically in Fig. 1(b), and is given by the familiar expression, $E_y(x,t) = E_{0y}\cos(\pi x/a)\cos(\omega t - k_{\parallel}z)$, $-a/2 \leq x \leq a/2$ where $a = 2.29$ cm equals the length of the wide dimension of the

4

waveguide. Therefore the probe designated $I_y(\text{EM})$ maps out primarily the RF profile associated with the electromagnetic wave launched into the interaction region. The fixed reference probe $I_y(\text{REF})$ likewise measures primarily the electromagnetic field intensity of the launched, amplified wave.

The right hand movable antenna, designated $I_x(\text{SC})$, is sensitive to the x component of any RF electric field. Cold tests indicate that because of slight misalignment, a small signal due to E_y is nonetheless present on this probe. However, this intensity is more than 25 dB below the intensity of the y component and thus causes no problems in the measurements described below.

During FEL activity, the presence of x-directed electric fields is due mainly to the quasi-electrostatic, irrotational fields of the bunched electrons, whose spatial distribution is illustrated schematically in Fig. 1(c). Higher order waveguide modes with electric field components in the x direction could also be present during FEL activity, but calculations show [12] that their expected amplitudes are very small compared with the space charge fields.

In addition to intensity profiles, we have also measured the profiles of the RF phase. This is accomplished by standard interferometric techniques [2]-[4] in which the antenna signal is mixed in a "magic tee" with a reference signal from the TWT launcher.

Typical oscilloscope traces of the intensity and phase are illustrated in Fig. 2. The FEL is fired by the discharging of the Marx accelerator. Because of an RC droop, the beam energy falls gradually as is illustrated in Fig. 2(a). Amplification [Fig. 2(b)], as measured by the y-oriented reference probe $I_y(\text{REF})$ occurs at a beam energy for which the slow (negative energy) space-charge wave on the beam is near phase synchronism with the electromagnetic wave. This results in the gain peak. The gain is ~ 3 dB. Later in time, at a lower beam energy, one observes a dip corresponding to wave absorption. Here the wave energy is converted to electron kinetic energy, as is known to occur when the fast (positive energy) space-charge wave is in synchronism with the electromagnetic wave.

The resonance relationship between the guided electromagnetic wave and the wave on the beam is given by the well known expressions

$$\omega^2 = c^2 k_{\parallel}^2 + \omega_c^2 \tag{1}$$

5

and

$$\omega = (k_{\parallel} + k_w)\beta_{\parallel}c \pm p_1\omega_p\phi^{1/2}/\gamma_{\parallel}\gamma^{1/2}, \tag{2}$$

where the plus sign corresponds to the fast, positive energy, "passive" space charge wave, and the minus sign corresponds to the slow, negative energy, "active" space charge wave; $\omega_c^2 = \omega_{c0}^2 + p_2\omega_p^2/\gamma$ is the effective waveguide cutoff frequency adjusted for the presence of the electron beam; ω_{c0} is the empty waveguide cutoff frequency [(in our case the lowest mode of a rectangular waveguide (TE_{10})]; $k_w = 2\pi/l_w$ is the wiggler wavenumber; $\beta_{\parallel} = v_{\parallel}/c$ is the normalized axial velocity of the electron beam, and $\omega_p = (Ne^2/m_0\epsilon_0)^{1/2}$ is the nonrelativistic plasma frequency. The relativistic mass increase $\gamma = 1 + eV/m_0c^2$ measures the beam energy; ϕ is the adjustment [13] to the plasma frequency due to the combined wiggler and axial magnetic fields; p_1 is the reduction in the plasma frequency that results from finite radial effects, and p_2 is the electromagnetic wave energy weighted ratio of the electron beam cross-section and the waveguide area. In normal operation of our FEL, $p_2 \approx 0.06$ so that $\omega_c \approx \omega_{c0}$, $p_1 \approx 0.5$, and $\phi \approx 1$.

Fig. 2(c) shows the corresponding oscilloscope trace as observed with the space charge probe $I_x(SC)$. As expected, it shows maximum activity at times when the electromagnetic wave interacts either with the slow or fast space charge waves.

Fig. 2(d) shows the temporal behavior of the RF phase of the electromagnetic wave. It is noteworthy that maximum phase change occurs at a time when the gain is close to zero, as is characteristic of FELs operating in the collective (Raman) regime [2].

In order to check the validity of these results, we dump the electron beam into the waveguide walls by means of a magnetic kicker placed 18 cm upstream of the probes. This allows the FEL-induced profile modification of the RF field to convert down to the fundamental TE_{10} mode, and null signals result (the higher modes excited by the FEL interaction are evanescent and die out exponentially within 1 or 2 waveguide wavelengths from the kicker position).

The experiments described below are carried out on electron beams with energy ranging from 150-170 keV and a current of ~1 A. The axial guide magnetic field is held constant

6

at 1580 G. The wiggler field amplitude is set at one of two values, 130 G and 200 G. The RF input signal has a frequency of 9.7 GHz and a power level of 3 W. With these parameters, the FEL operates in the linear regime and has a single pass gain of $\sim$ 3 dB at the axial position $z \approx 115$ cm from the beginning of the wiggler, where the antennas are located.

3. SPACE-CHARGE FIELD PROFILES

The spatial distribution of the DC current density $J_z(x, y)$ of the electron beam is determined by using the space charge dipole antenna (designated $I_x(\text{SC})$ in Fig. 1) as a current monitor. This is accomplished by terminating the coaxial cable from the antenna with a 50 Ohm load and measuring the voltage across it. Figure 3(a) illustrates the current density profile $J_z(x, 0)$ as a function of displacement of the antenna in the x direction. We see that the full width of the distribution at half maximum is $\sim$5 mm, and equals the diameter of the emittance selector placed upstream from the wiggler. Figure 3(b) shows the current density distribution $J_z(0, y)$ as a function of displacement in the y direction. This measurement is carried out by holding the antenna position fixed at $x = 0, y = 0$ and moving the entire waveguide in the y direction relative to the stationary electron beam. This determination is of course less accurate because of the considerable loss of symmetry caused by the waveguide displacement relative to the beam. The above measurements of the beam size and beam center are needed in understanding the subsequent RF intensity profiles.

To use the space-charge probe $I_x(SC)$ for the measurement of the RF fields, the DC beam current is shunted to ground, the RF field is rectified by a crystal diode and then displayed on a fast oscilloscope. Figure 4(a) illustrates how the electric field intensity $I_x(x, 0)$ of the space charge wave varies as a function of the probe displacement in the x direction. We see that $I_x(x, 0)$ is zero at the center of the electron beam, is maximum near the beam edge $x = r_b$ and falls off rapidly when $|x| > r_b$, in agreement with the expected behavior of the irrotational fields produced by the bunched electron beam. Figure 4(b) shows the variation in $I_x(0, y)$ as the antenna traverses the beam center in the y direction; and $I_x(r_b, y)$ gives the intensity variation as it traverses the beam edge. The small cartoons in the upper right hand corner illustrate schematically the motions of the space charge

7

probe. We note that these fields exist only during FEL activity, and become immeasurably small when, for example, the wiggler field is turned off or when the resonance conditions (1) and (2) are not fulfilled.

Combining data like that illustrated in Figure 4, one can generate a two-dimensional plot of the space charge field intensity profile. This is shown in Figure 5.

Since the space charge electric field points radially outwards from the electron beam center, it must undergo a 180° phase change in traversing the center. This effect is illustrated in Figure 6. Figure 6(a) shows a plot of the phase of the space charge wave as a function of time during the falling voltage pulse for two discrete positions of the antenna on opposite sides of the centre $x = \pm 4$ mm. Figure 6(b) gives the phase as a function of the antenna displacement in the x direction at a time during the pulse when the phase change is maximum (and the gain is near zero). It shows clearly the abrupt phase change when the beam center is crossed. This correct phase behavior also lends strong support to the validity of the observations of Figs. 2, 4 and 5, when the antennas are used in intensity measurements.

4. ELECTROMAGNETIC WAVE PROFILES

In this section we describe intensity and phase measurements using the movable antenna $I_y(EM)$ of Fig. 1. This antenna is oriented orthogonally to the space charge antenna $I_x(SC)$ of section 3, and is sensitive to electric fields E_y parallel to the direction y of the launched TE_{10} electromagnetic wave. In the absence of FEL activity measurements show that $I_y(EM)$ varies as $cos^2(\pi x/a)$ in accordance with expectations. This has been found to be so both in the absence of the electron beam (cold tests), and also in its presence, provided that the relevant FEL parameters were far removed from the resonance conditions (1) and (2).

In the presence of FEL activity the electric field intensity profile measured with antenna $I_y(EM)$ can be modified by one of two effects: optical guiding and contribution from the ambient space charge field $E_y(SC)$ of the bunched beam. Figure 7 illustrates the extent to which the RF profile is altered. In plotting the percentage change as a function of displacement, we subtract the underlying $cos^2(\pi x/a)$ variation.

8

The very substantial changes shown in Fig. 7 are in agreement with earlier measurements [14]. There, the observations were attributed to optical guiding. However, in view of the now available space charge field measurements of section 3 and recent theoretical input [12], [15] the earlier interpretation needs closer scrutiny. The point is, that the $I_y(EM)$ probe measures a signal that is proportional to $|E_y(EM)cos(\omega t - k_{\parallel}z) + E_y(SC)cos(\omega t - (k_{\parallel} + k_w)z)|^2$ which, after time averaging, consists of a sum of intensities $E_y^2(EM) + E_y^2(SC)$, and an interference term $2E_y(EM)E_y(SC)cos(k_w z)$. And, even if $E_y^2(SC) \ll E_y^2(EM)$, the interference term can produce significant profile modifications.

To be sure, the space charge electric fields are zero at the electron beam center and are large only near the beam edge $x = \pm r_b, y = \pm r_b$ (see Figs. 1, 4 and 5). Also, $E_y(SC)$ is by symmetry exactly zero along the x axis. Along the x axis, $E_y(SC)$ should not contribute to the overall intensity, were it not for the fact that the antenna has a finite length in the y direction(~ 1 mm) and it can therefore pick up a small amount of y component of the space charge electric field. As a result, some contribution from $E_y(SC)$ occurs even along the x axis.

We have also carried out a series of measurements with the purpose of determining the relative amplitudes of the space charge and electromagnetic fields. We find that at spatial positions where each are at their maximum, the ratio $E_{SC}(r = r_b)/E_{EM}(r = 0) \approx 0.2$. This yields a value for the interference term whose magnitude is not inconsistent with the profile modifications shown in Fig. 7. To confirm this, we displaced the antennas axially by exactly half a wiggler period [such that $z' = z + l_w/2$] and performed a profile scan. The result is illustrated in Fig. 8. Comparing Figs. 7 and 8 we see that the profile "flipped over", an effect which must be attributed to a sign change in the interference term $2E_y(EM)E_y(SC)cos(k_w z)$. A scan of the phase shown in Fig. 9 exhibits a similar effect.

5. DISCUSSION

This paper is an experimental study of the quasi-electrostatic and electromagnetic fields, and their relative importance, generated during FEL activity. The experiments were performed in a Raman free electron laser under conditions where the collective effects due to the RF space charge cannot be neglected.

9

Section 3 is devoted to the study of the RF intensity and phase of the space charge fields. The spatial distribution of the transverse field component $E_x(SC)$ represents essentially the fringe fields of the space charge bunches generated during FEL activity. These fields vanish on the z axis and are antisymmetric, as is clearly demonstrated by Figs. 4, 5 and 6.

In section 4 we examine the transverse spatial profiles of the electromagnetic wave. The observed modification (Fig. 7), though originally believed to be due to optical guiding [14], is now ascribed to the presence of a small but not insignificant contribution from the space charge fields of the bunches. The space charge wave travels at a somewhat slower speed than the electromagnetic wave and the two waves are phase-locked to one another. This gives rise to wave interference, and to profiles like those shown in Fig. 7. A dramatic example of this interference effect is illustrated by comparing these profiles with those of Fig. 8, which were measured at a second axial position Z' displaced one half a wiggler period downstream. Phase measurements of Fig. 9 provide additional confirmation of the interference phenomenon. Any true optical guiding of the electromagnetic wave that may be present is masked by interference effects with the space charge wave.

Interference among the several [15] waves generated in an FEL interaction is also believed to be the cause of the following interesting effect that we have observed in the course of our measurements. Oscilloscope traces like those illustrated in Fig. 2(b) exhibit an overall temporal shift as a function of the transverse position x of the antenna used on making the measurement. This is shown in Fig. 10(a) in which the $I_y(EM)$ probe, positioned at different transverse positions, is used in the measurement of the RF output. We see that as $|x|$ increases, the gain peak as well as the absorption dip move to later times, that is, to lower electron beam energies γ. We ascribe this to wave interference among the several interacting waves [15] each characterized by slightly different detuning parameters $\delta(x) = \omega/v_{||} - k_{||}(x) - k_w$ and different transverse wave profiles. When the gain is low (~ 3 dB), as it is in our experiments, all interacting waves carry roughly the same weight. The observed temporal changes can be translated into corresponding changes in the beam energy parameter γ. This is illustrated in Fig. 10(b), where we plot the beam energy for maximum FEL gain, $\gamma_{max}(x)$, as a function of the transverse antenna position

z.

In conclusion, then, the experimental observations presented in this paper can serve as a basis for a detailed theoretical study of profile modifications in a Ramam FEL. To date, the theoretical analyses are in qualitative agreement with our measurements. However, there are large numerical differences. For example, theory predicts [12] that the ratio of the space charge to the electromagnetic field amplitude is ~ 0.02 which is about an order of magnitude smaller than the measured ratio. Similarly, the predicted change [15] in the temporal pattern as a function of transverse position x is much smaller than that obtained from the measurements like those shown in Fig. 10.

AKNOWLEDGEMENTS

REFERENCES

[1] P. Sprangle, R. A. Smith, and V. L. Granatstein, Infrared and Millimeter Waves, edited by K. J. Button (Academic, New York, 1979), Vol. 1, p. 279, and references therein. also N. M. Kroll, and W. A. McMullin, Phys. Rev. A17, 300 (1978).

[2] J. Fajans and G. Bekefi, Phys. Fluids 29, 3461 (1986).

[3] J. Fajans, J. S. Wurtele, G. Bekefi, D. S. Knowles, and K. Xu, Phys. Rev. Lett. 57, 579 (1986).

[4] T. J. Orzechowski, E. T. Scharlemann, and B. D. Hopkins, Phys. Rev. A 35, 2184 (1987).

[5] P. Sprangle and C. M. Tang, Appl. Phys. Lett. 39, 677 (1981).

[6] W. M. Kroll, P. L. Morton, and M. W. Rosenbluth, IEEE J. Quantum Electron. 17, 1436 (1981).

[7] J. M. Slater and D. D. Lowenthal, J. Appl. Phys. 52, 44 (1981).

[8] D. Prosnitz, A. Szoke, and V. K. Neil, Phys. Rev. A 24, 1436 (1981); also D. Prosnitz, R. A. Haas, S. Doss, and R. J. Gelinas, in *Free Elecctron Generators of Coherent Radiation*, Physics of Quantum Electronics Vol. 9, edited by Stephen F. Jacobs, Murray Sargent, III, and Marlan O. Scully (Addison-Wesley, Reading, MA, 1982), p. 1047.

[9] E. T. Scharlemann, A. M. Sessler, and J. S. Wurtele, Phys. Rev. Lett. 54, 1925 (1985).

[10] G. T. Moore, Opt. Commun. 52, 46 (1984), and Nucl. Instrum. Methods Phys. Res. Sect. A 239, 19 (1985).

[11] J. Fajans, J. Appl. Phys. 55, 43 (1984).

[12] E. Jerby and A. Gover (to be published in Phys. Rev. Letters).

[13] H. P. Freund and P. Sprangle, Phys. Rev. A 28, 1835 (1983).

[14] F. Hartemann, K. Xu, G. Bekefi, J. S. Wurtele and J. Fajans, Phys. Rev. Lett. 59, 1177 (1987).

[15] J. Fajans and J. S. Wurtele (to be published in Phys. Fluids).

FIGURE CAPTIONS

Figure 1 Schematic diagram of the experimental arrangement showing the placement of the probing antennas.

Figure 2 Oscilloscope traces of (a) the beam voltage; (b) RF field intensity of the electromagnetic wave; (c) intensity of the space charge wave; and (d) RF phase of the electromagnetic wave (see text). The straight lines in (b), (c) and (d) are traces when the beam is kicked out of the system 18 cm upstream from the antennas, thereby terminating FEL activity at that point. The experimental parameters are: $B_{||} = 1580$ G; $Bw = 130$ G; $\omega/2\pi = 9.7$ GHz; $I \simeq 1$ A; RF power input= 3 W.

Figure 3 DC current density profile $J_z(x,y)$ of the electron beam, measured at the position of the dipole antennas.

Figure 4 Transverse field intensity profiles of the space charge (ponderomotive) wave of the bunched electron beam at a time of maximum FEL gain. The cartoons in the upper right hand corner illustrate the directions of scan. The experimental parameters are the same as in the caption to Fig. 1 except that $B_w = 200$ G, $I \simeq 4$ A.

Figure 5 Two dimensional presentation of the transverse field intensity profile of the space charge wave at a time of maximum FEL gain. The experimental parameters are the same as in Fig. 4.

Figure 6 Transverse phase profile of the space charge wave at a time of maximum phase change (a) as a function of time during the voltage pulse; (b) as a function of antenna position at a time near zero gain (see text). The experimental parameters are the same as in Fig. 4.

Figure 7 Two dimensional distribution of $I_y(EM)$ (the normalized electromagnetic wave intensity) at an axial position $z \simeq 115$ cm and at a time of maximum gain. The experimental parameters are the same as in Fig. 2.

Figure 8 Two dimensional distribution of $I_y(EM)$ (the normalized electromagnetic wave intensity) at an axial position $z' = z + l_w/2$ and at a time of maximum gain. The experimental parameters are the same as in Fig. 2.

Figure 9 Phase distribution as a function of transverse displacement at a time of maximum

phase change (near zero gain) at (a) $z = 115$ cm and (b) $z' = z + l_w/2$. The experimental parameters are the same as in Fig. 2.

Figure 10 (a) Oscilloscope traces (cf Fig. 2) of the beam voltage and of the intensity $I_y(EM)$ for 4 different positions x of the probing antenna, showing overall pattern shift to lower voltages. (b) beam energy parameter $\gamma_{max}(x)$ at maximum gain as a function of the axial displacement x.
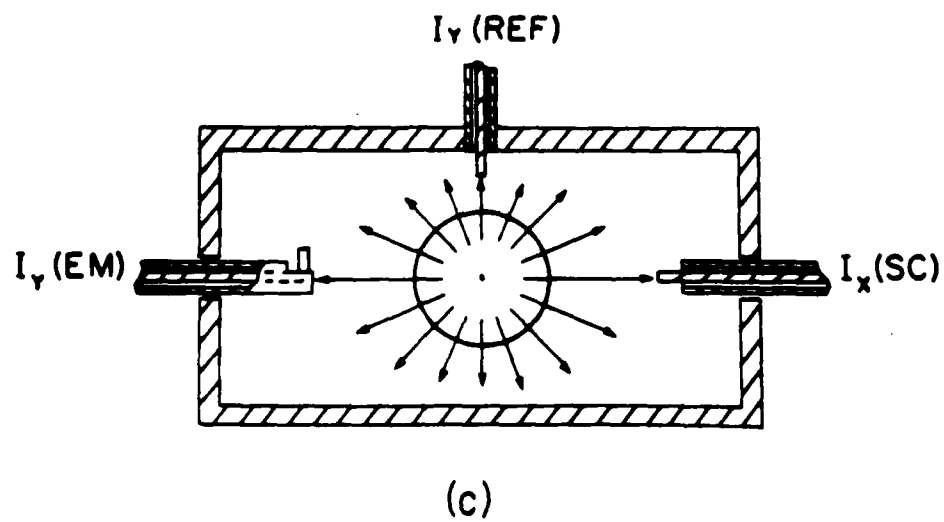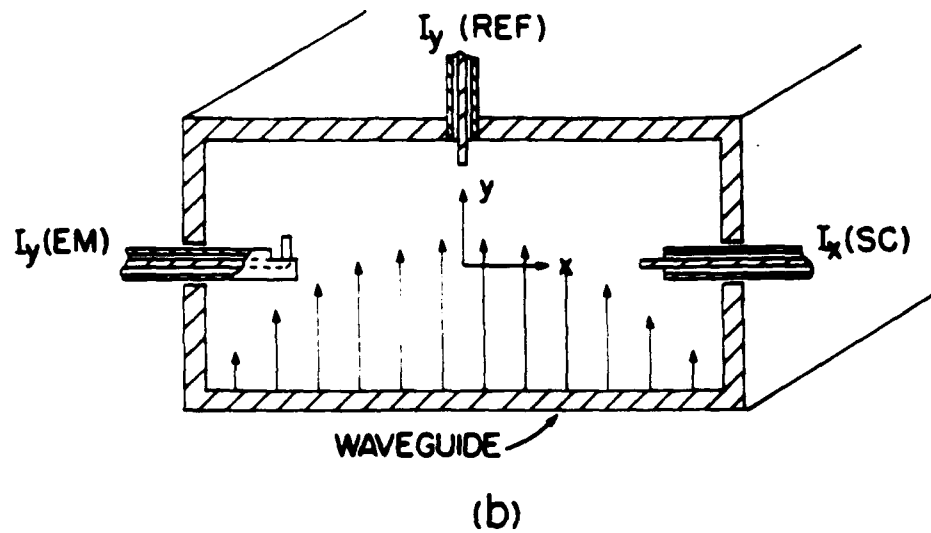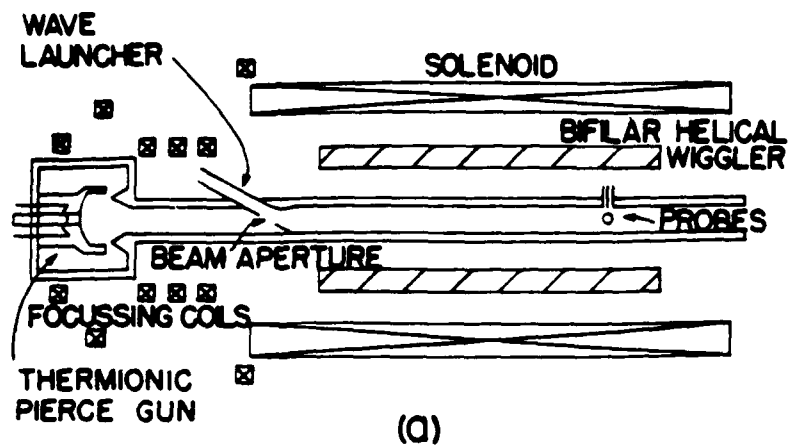
WAVE
LAUNCHER

SOLENOID

BIFILAR HELICAL
WIGGLER

PROBES

BEAM APERTURE

FOCUSSING COILS

THERMIONIC
PIERCE GUN

(a)

I_y (REF)

I_y(EM)

I_x(SC)

y

x

WAVEGUIDE

(b)

I_y (REF)

I_y (EM)

I_x(SC)

(c)

Fig.1   Xu,Bekefi,Leibovitc
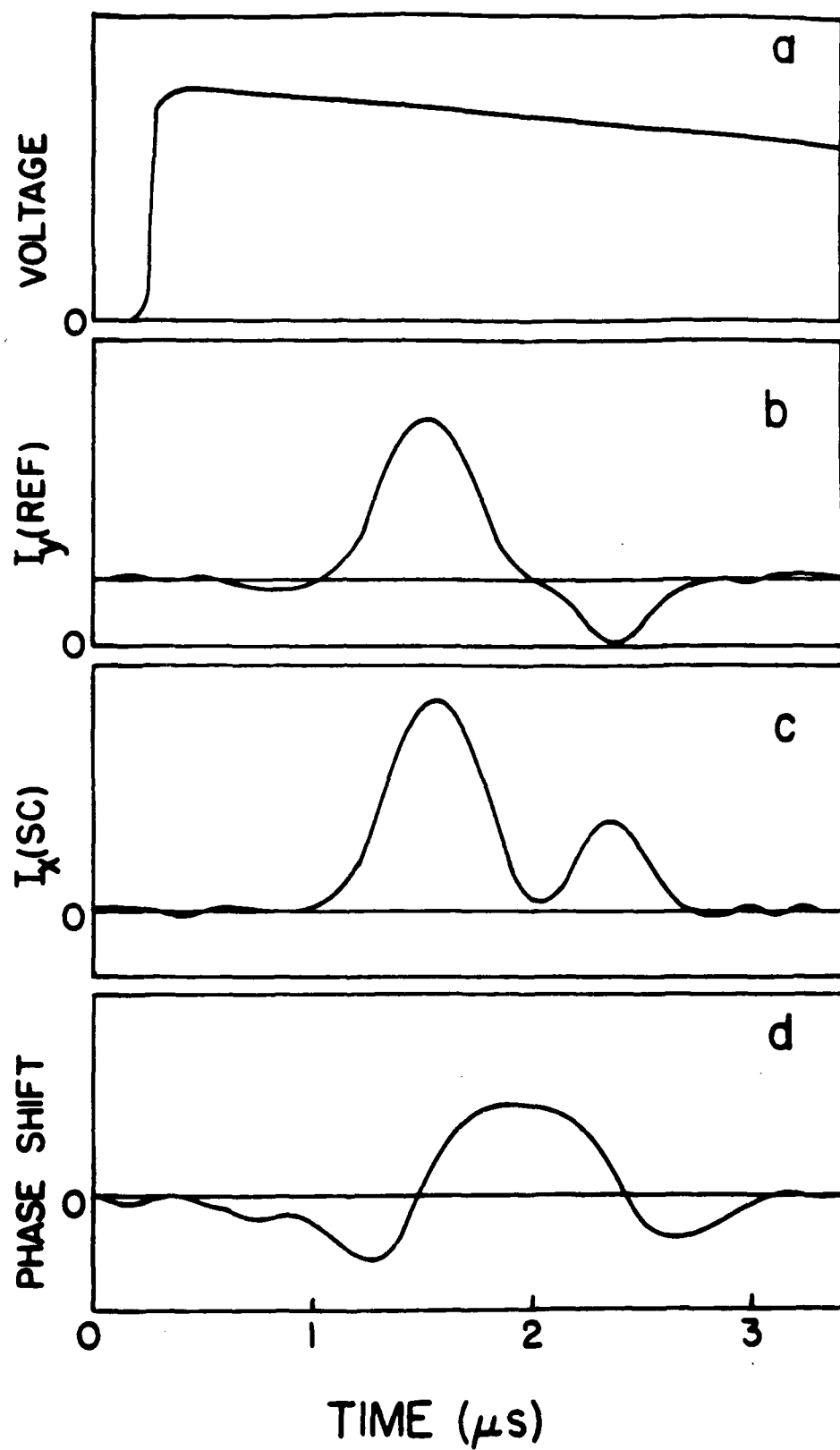
Fig.2   Xu,Bekefi,Leibovitե

Fig.3 Xu,Bekefi,Leibovit

(a)

INTENSITY I_x(SP) [REL. UNITS]

DISPLACEMENT IN X DIRECTION (mm)

(b)

INTENSITY I_x(SP) [REL. UNITS]

DISPLACEMENT IN Y DIRECTION (mm)

Fig.4   Xu,Bekefi,Leibovitch

PHASE

x = -4 mm

x = +4 mm

(a)

TIME (μS)

PHASE (DEGREES)

180

0

BEAM

(b)

DISPLACEMENT IN X DIRECTION (mm)
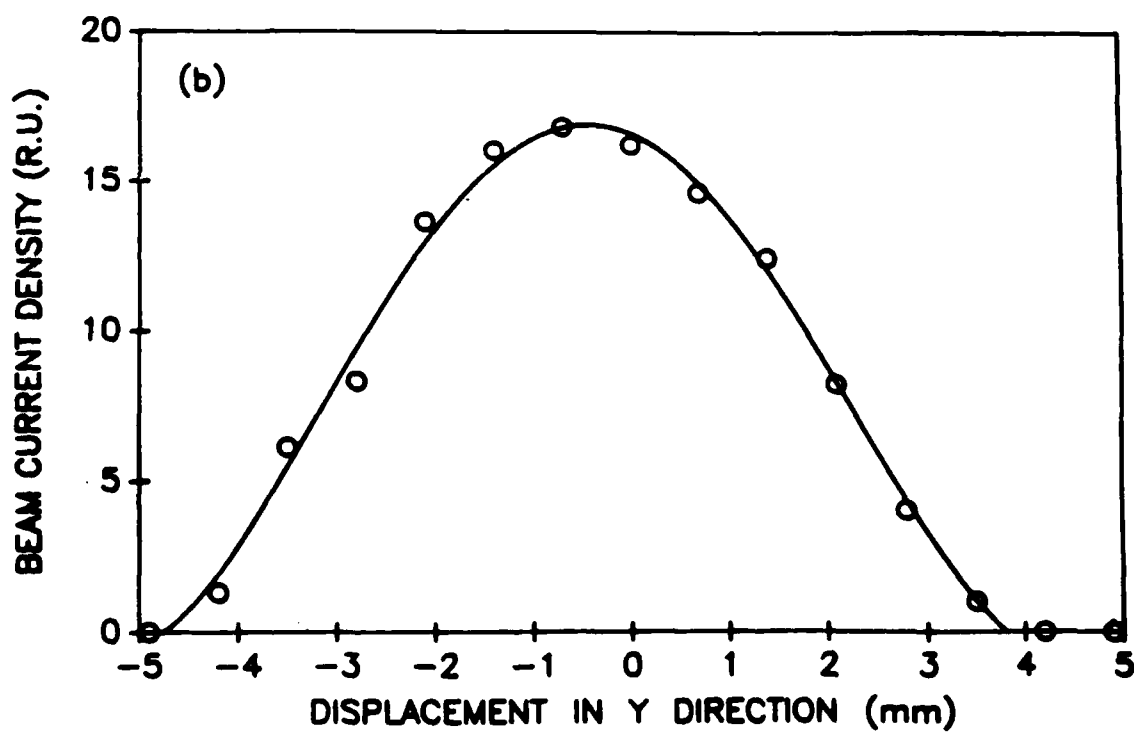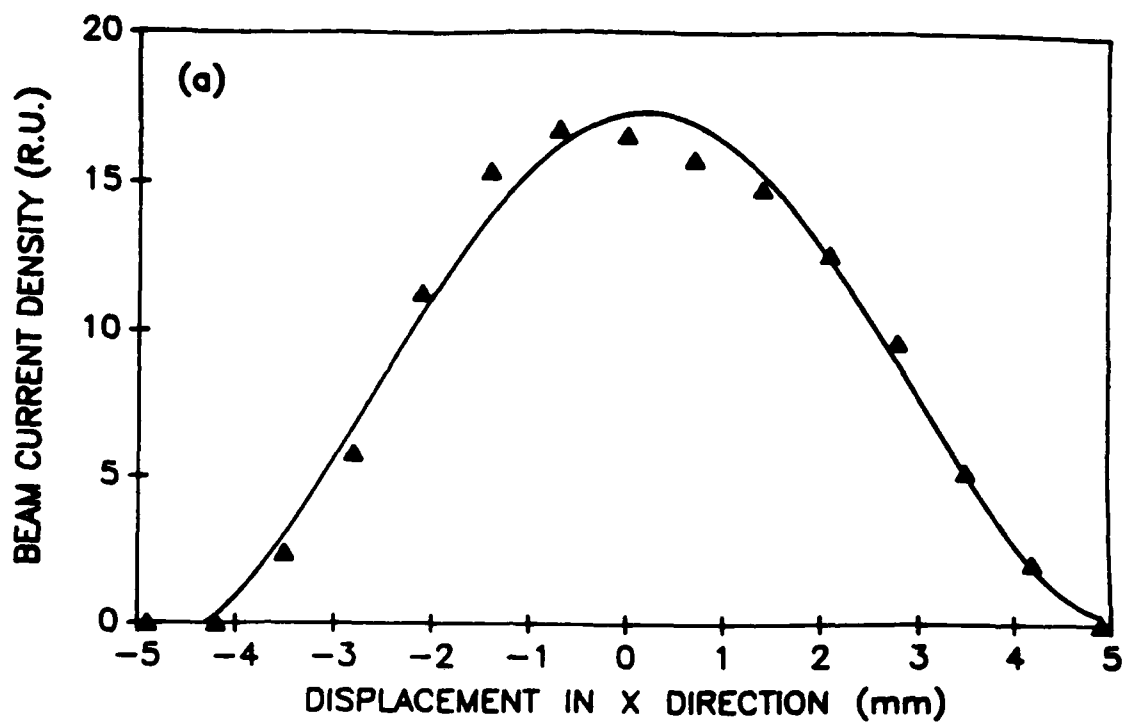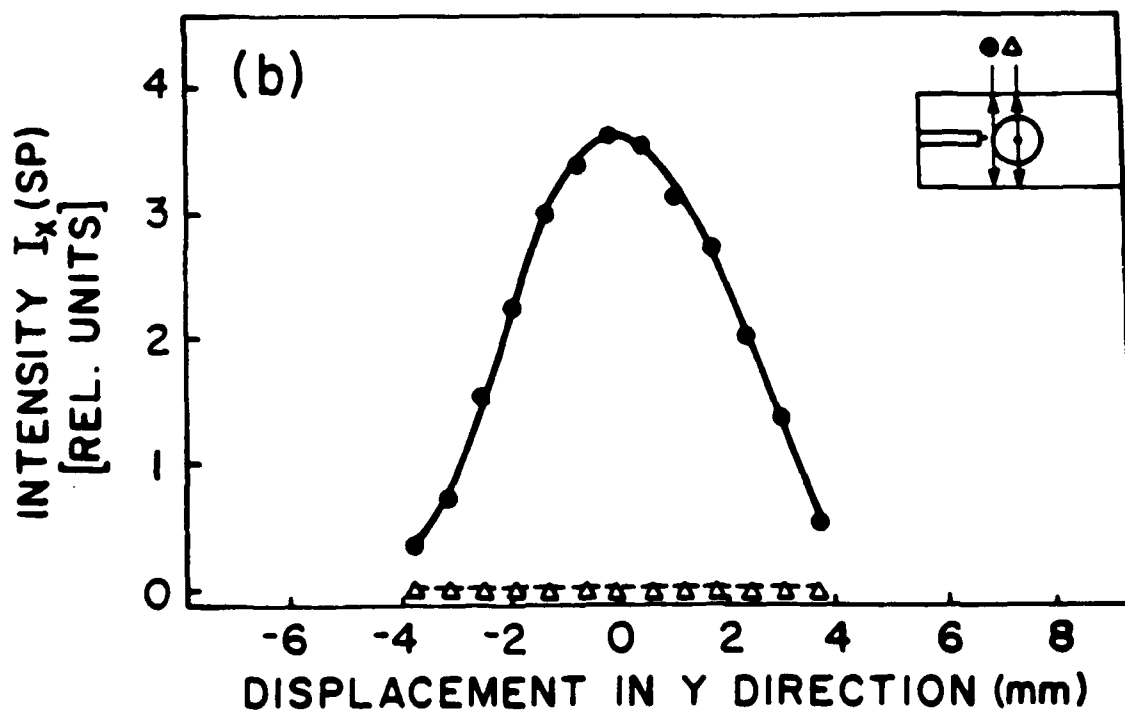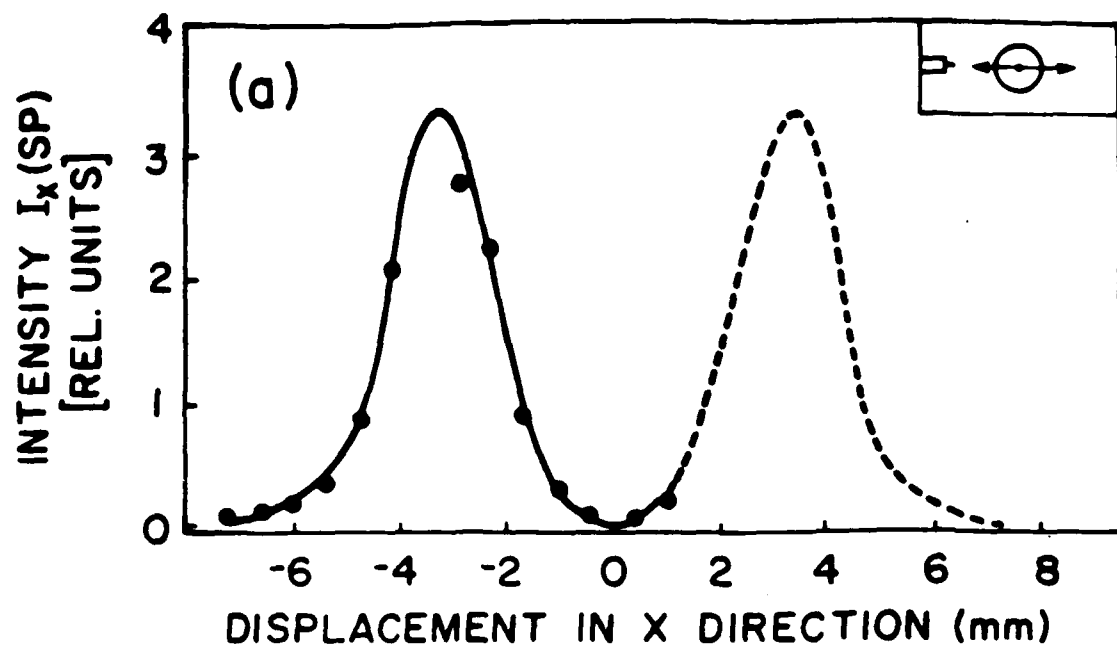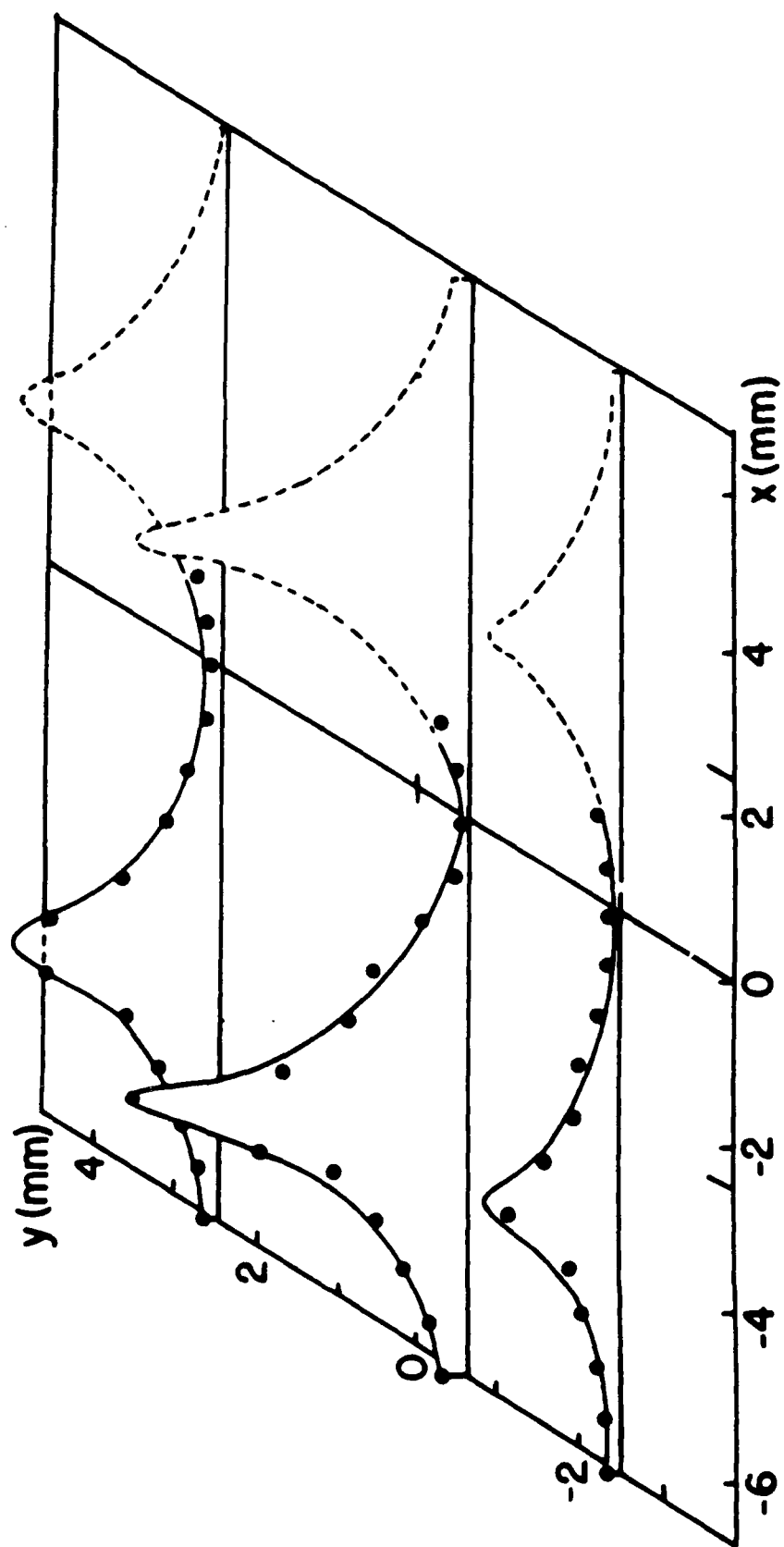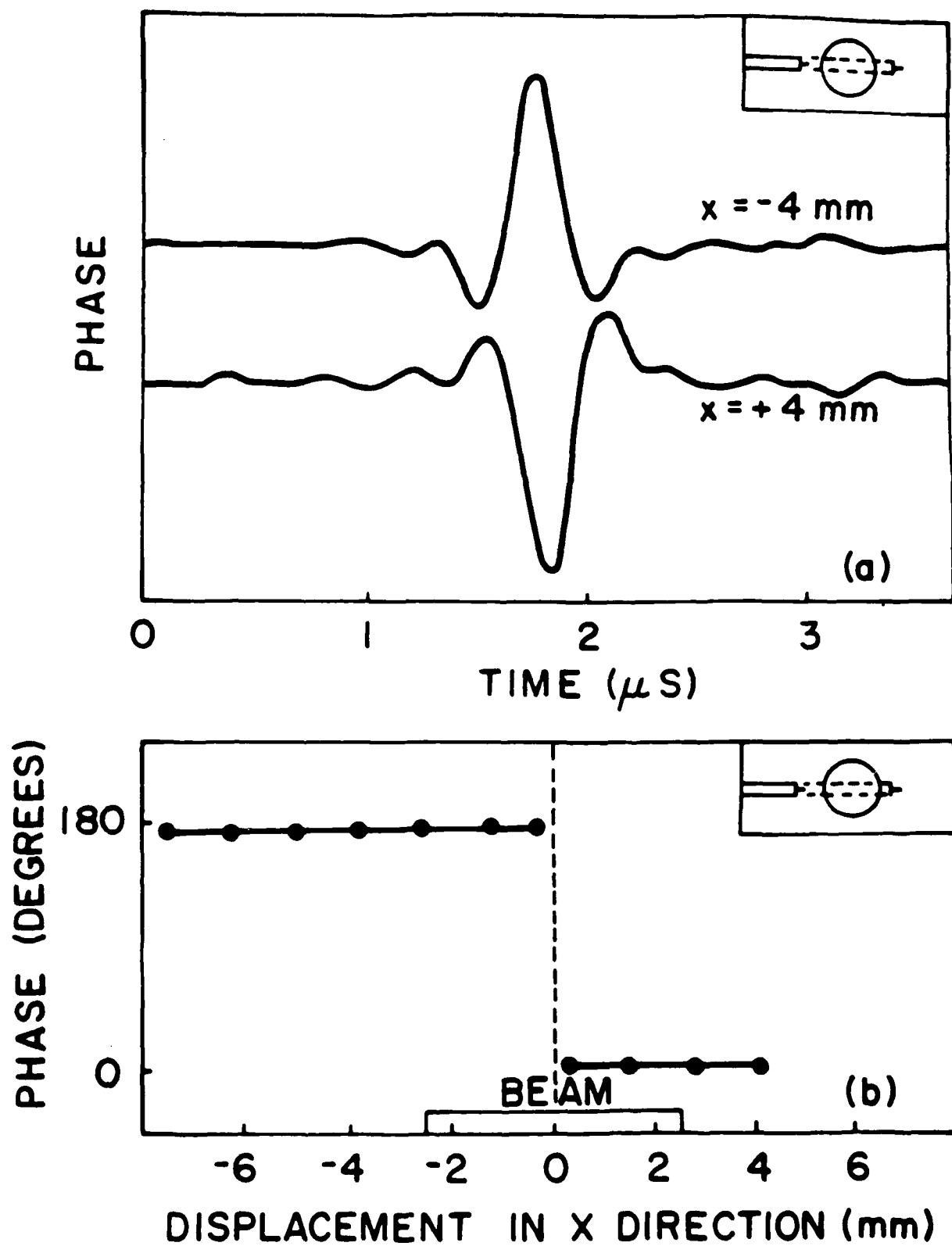
Fig.6 Xu,Bekefi,Leibovitch

Fig. 8. Yu Rakoti Lothavitch

NORMALIZED
INTENSITY

y (mm)

x (mm)

Fig.9 Xu,Bekefi,Leibovi
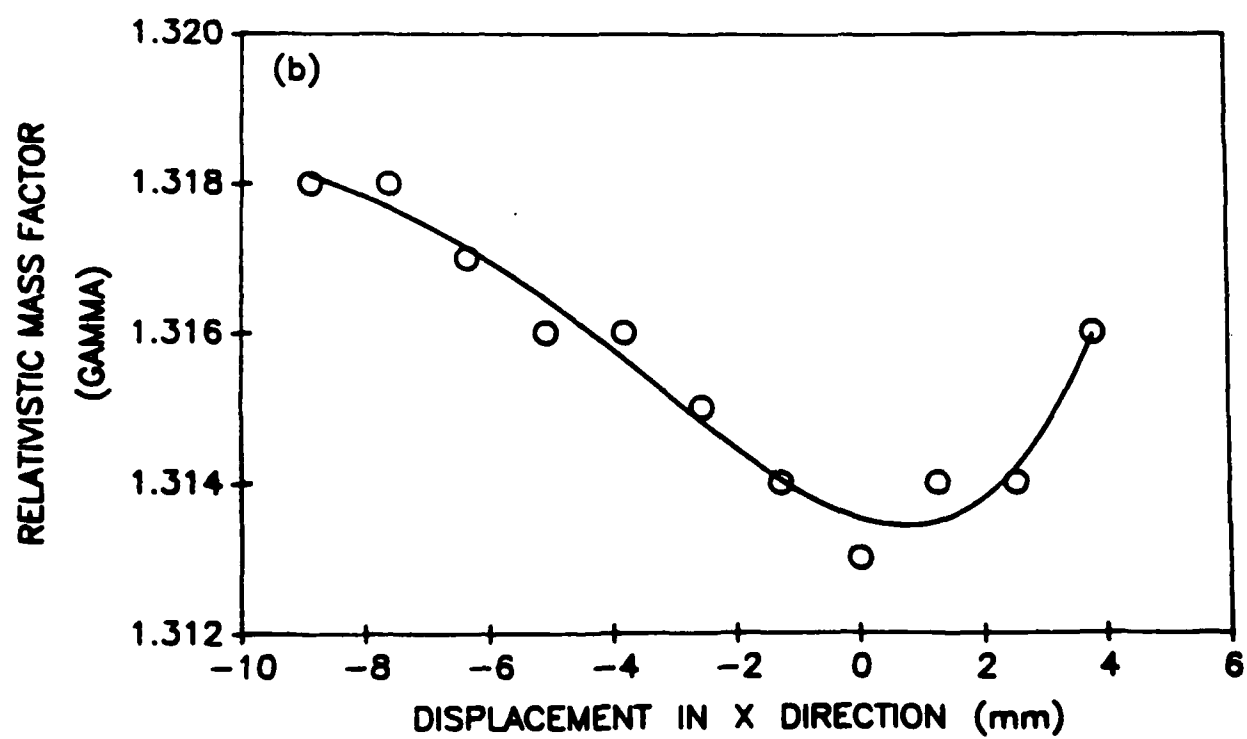
(a)

VOLTAGE

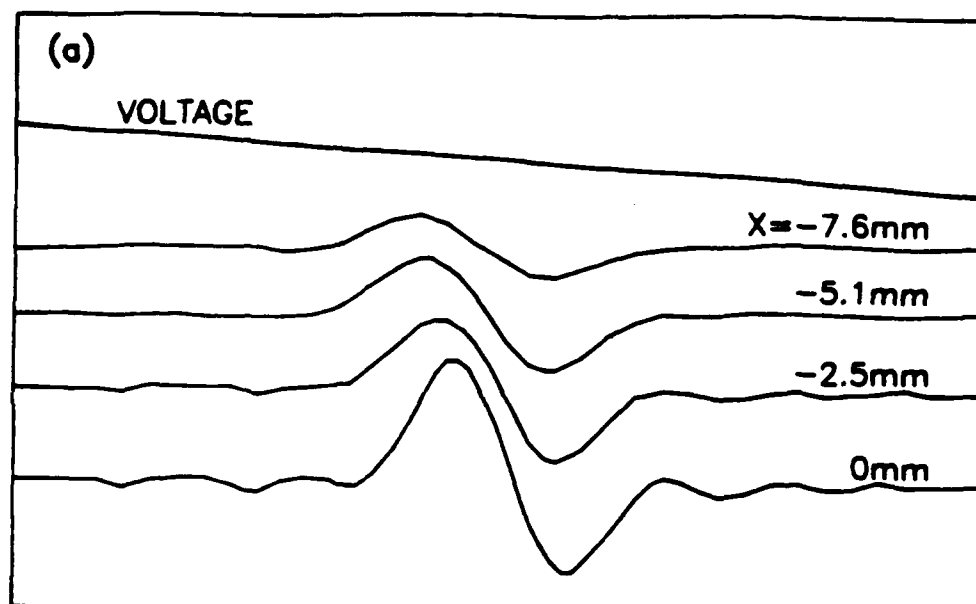X = -7.6mm

-5.1mm

-2.5mm

0mm

(b)
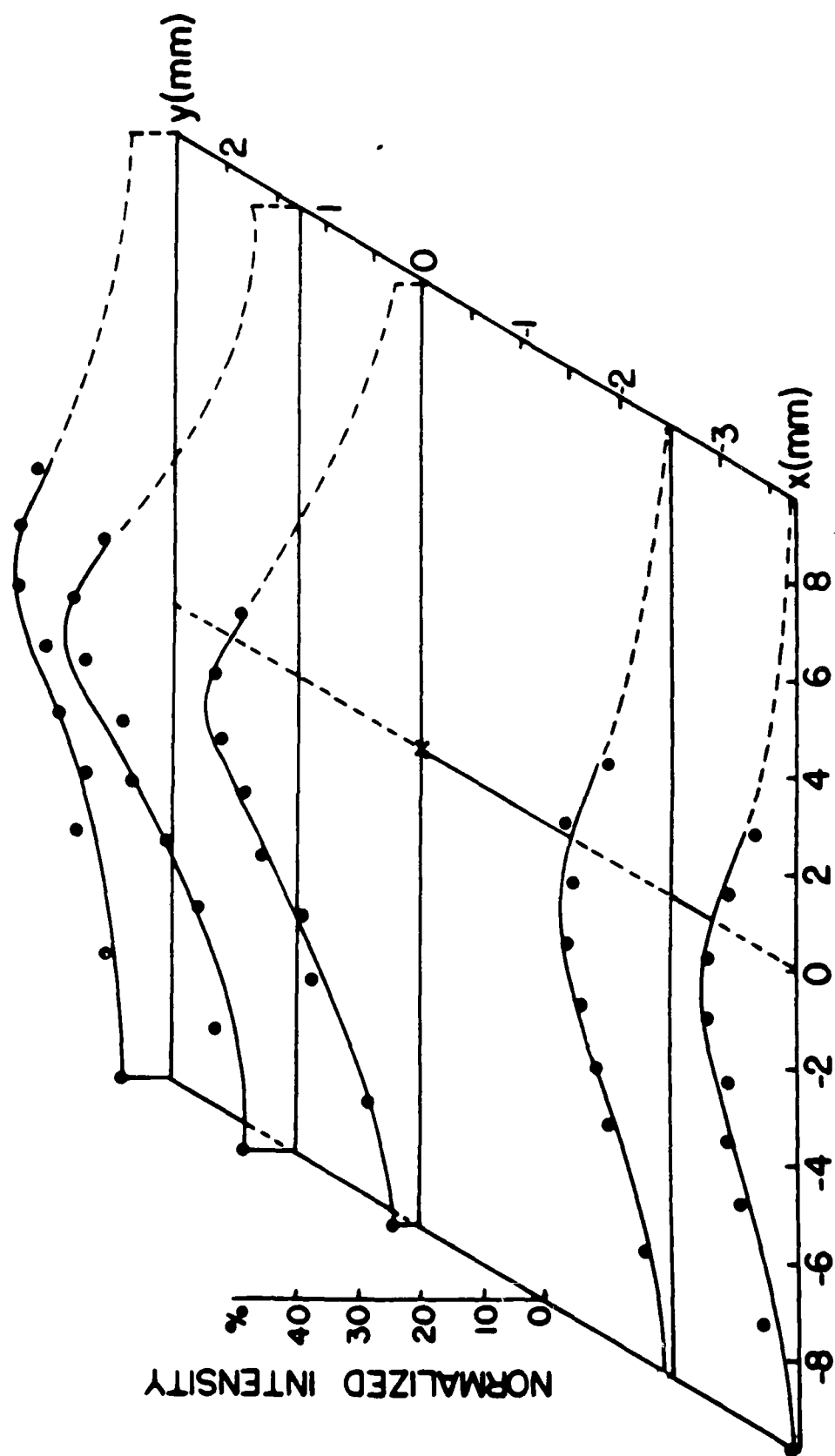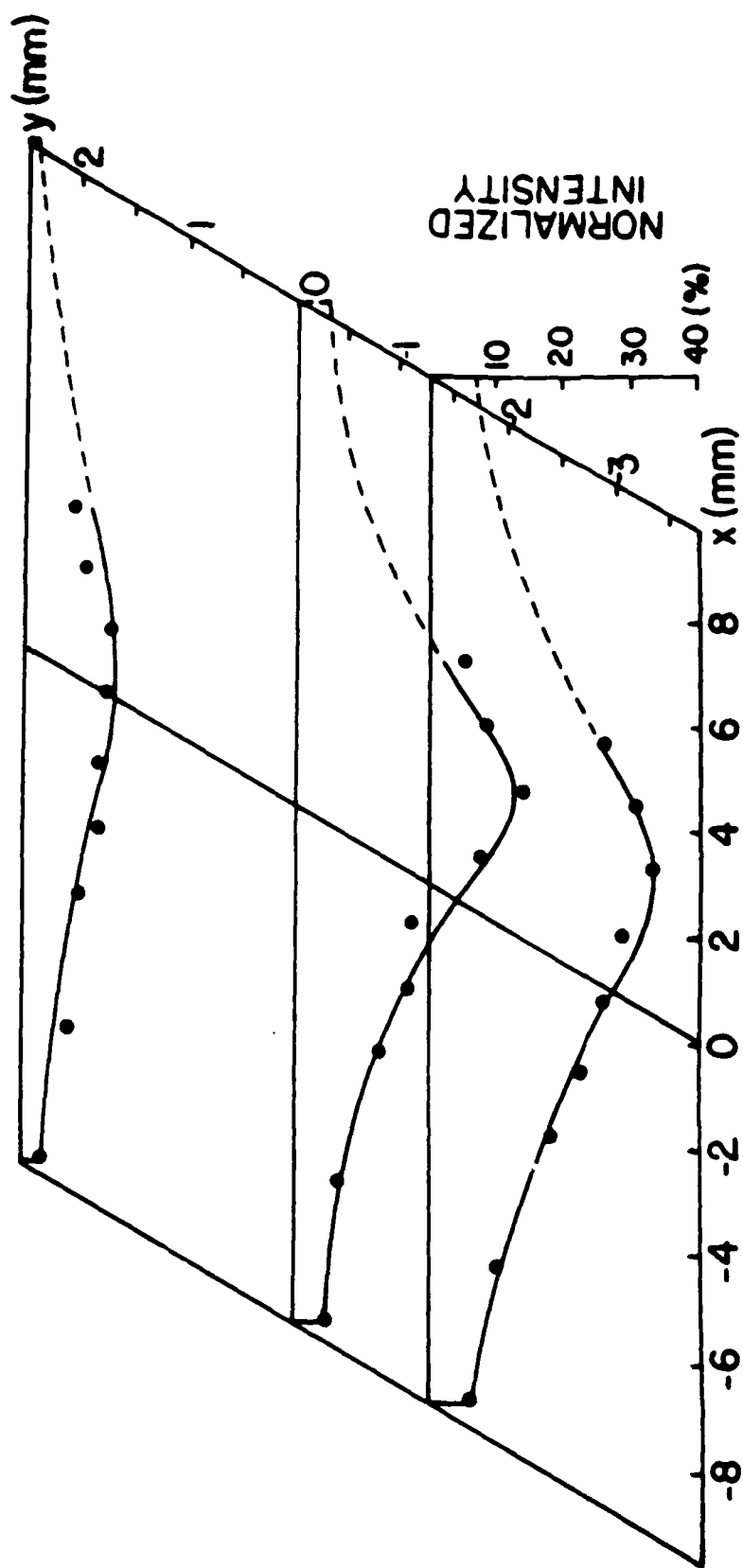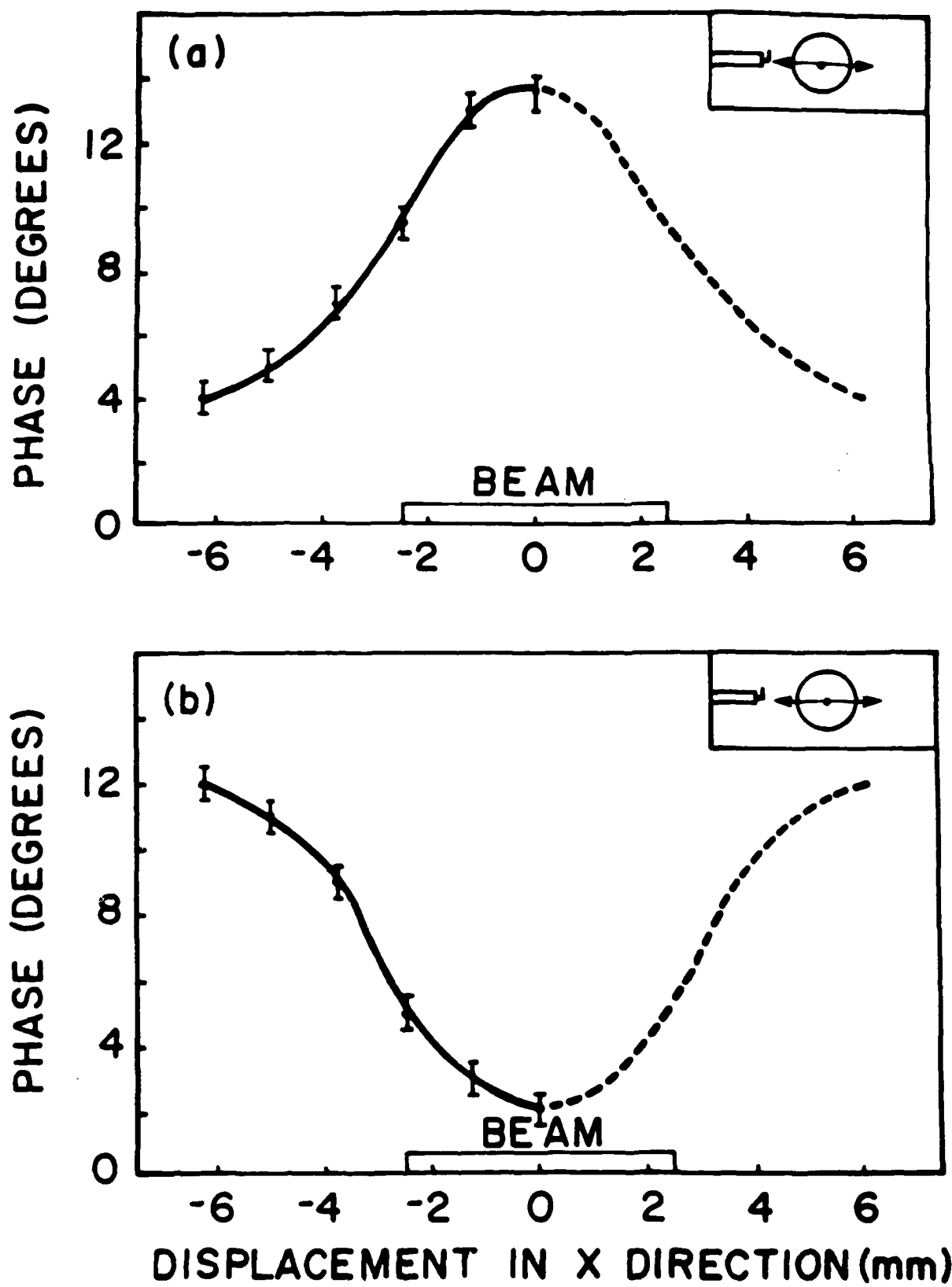
Fig.10 Xu,Bekefi,Leibovitch

Appendix 2

A 35 GHz CYCLOTRON AUTORESONANCE MASER AMPLIFIER

G. Bekefi, A. DiRienzo, C. Leibovitch and B.G. Danly

Department of Physics,
Research Laboratory of Electronics
and
Plasma Fusion Center
Massachusetts Institute of Technology
Cambridge, Massachusetts 02139

Abstract

Studies of a cyclotron autoresonance maser are presented. The measurements are carried out at a frequency of 35 GHz using a mildly relativistic electron beam (1.5 MeV, 260 A) generated by a field emission electron gun followed by an emittance selector that removes the outer, hot electrons. Perpendicular energy is imparted to the electrons by means of a bifilar helical wiggler. Measurements give a small signal gain of 90 dB/m and a saturated power output of 10 MW. The corresponding electronic efficiency is 3%. Computer simulations are also presented.

1

The cyclotron autoresonance maser (CARM) has been subjected to extensive theoretical [1],[2] studies and numerical simulations [3]-[5]. However, unlike the gyrotron and the free electron laser, its capabilities as a source of coherent millimeter wavelength radiation remain virtually untested in the laboratory. To the best of our knowledge, only CARM oscillator experiments [6],[7] have been reported in the literature. We present here what we believe to be the first published studies of a CARM amplifier.

The emission from a CARM results through an interaction between the Doppler upshifted cyclotron wave on the electron beam

$$\omega = \Omega_0/\gamma + k_\parallel v_\parallel \tag{1}$$

and an electromagnetic waveguide mode

$$\omega^2 = k_\parallel^2 c^2 + \omega_c^2; \tag{2}$$

ω and $k_\parallel$ are the frequency and axial wavenumber repectively; $\Omega_0 = eB_\parallel/m$ is the non-relativistic electron cyclotron frequency associated with an axial guide magnetic field $B_\parallel$: $\gamma = [1 - (v_\parallel/c)^2 - (v_\perp/c)^2]^{-1/2}$ is the relativistic energy factor; and ω_c is the cutoff frequency of the waveguide mode in question. Maximum gain of the CARM instability occurs near phase velocity synchronism of the two waves. This yields the radiation frequency:

$$\omega \simeq \Omega_0 \frac{\gamma_\parallel^2}{\gamma} \{1 \pm \beta_\parallel [1 - (\frac{\omega_c \gamma}{\Omega_0 \gamma_\parallel})^2]^{1/2}\} \tag{3}$$

Here $\beta_\parallel = v_\parallel/c, \gamma_\parallel = (1 - \beta_\parallel^2)^{-1/2}$, and the positive sign refers to the sought after Doppler upshifted CARM mode of operation.

A schematic of the CARM amplifier is shown in Fig. 1. The accelerator potential is supplied by a Marx generator (Physics International Pulserad 110 A) with a maximum capability of 1.5 MV and 20 kA. The electron beam is generated by a field emission gun composed of a hemispherical graphite cathode and conical anode, which also acts as an emittance selector. The entire two meter long system is immersed in a uniform solenoidal magnetic field of 7 kG.

The 260 A, 1.5 MV beam that issues from the emittance selector has a radius of 0.254 cm and a measured [8] normalized beam brightness equal to 2.4×10^4 A cm^{-2}rad^{-2}. This corresponds to a normalized root mean square emittance of 4.9×10^{-2} cm-rad and an RMS energy spread $\Delta\gamma_\parallel/\gamma_\parallel \simeq 0.019$. We note that considerably higher beam brightness is achieved by sacrificing current. When the radius of the the emittance selector is is reduced to 0.076 cm, the current drops to 8.4 A, but the brightness increases to 9.5×10^4

A cm^{-2}rad^{-2}. The corresponding emittance is now 4.5×10^{-3} and the energy spread $\Delta\gamma_{\parallel}/\gamma_{\parallel} \simeq 0.0017$.

The aforementioned 260 A electron beam is injected into a bifilar helical wiggler which imparts perpendicular energy to the electrons. The wiggler has a periodicity of 7 cm and is six periods long. Within the first 5.5 periods, the wiggler magnetic field increases slowly and thereby provides an adiabatic input for the electron beam; the last half period provides a uniform wiggler field with an amplitude on axis equal to 525 G. The resulting transverse electron velocity ($v_{\perp}$) is derived from witness plate observations of the beam precession as a function of axial position, giving $v_{\perp}/c = 0.30 \pm 0.05$.

The downstream end of the wiggler is terminated abruptly by means of a metal shorting ring and the spinning electrons are allowed to drift into the 100 cm-long CARM interaction region where they are subjected to the uniform axial magnetic field only. We note that as a result of the wiggler excitation and the abrupt wiggler termination, the energy spread $\Delta\gamma_{\parallel}/\gamma_{\parallel}$ of the electrons entering the CARM region can be considerably worse than the energy spreads quoted above in reference to electrons leaving the emittance selector. At the present time we have no way of measuring directly the beam energy spread at the entrance into the CARM region.

The $\sim$ 2m long, 0.787 cm radius evacuated drift tube acts as a cylindrical waveguide whose fundamental TE_{11} mode has a cutoff frequency $\omega_c/2\pi = 11.16$ GHz. Fig. 2 illustrates the time history of the voltage, current and radiation characteristics of the device. The CARM has been operated both in the superradiant mode, in which the signal is allowed to grow out of background RF noise, and as an amplifier.

At the output end of the CARM, a mica window transmits the circularly polarized radiation generated in the drift tube, where it is measured by means of standard calibrated crystal detectors, and its spectrum is analyzed by means of a 98m-long dispersive line. In the superradiant mode of operation, two spectral features are observed having differing tuning characteristics with axial magnetic field $B_{\parallel}$. In the frequency range of 30-45 GHz available to us, the frequency of the stronger spectral line increases linearly with $B_{\parallel}$ as predicted by Eq. 1. The weaker line is rather insensitive to $B_{\parallel}$. We think that this line may represent the second harmonic of the Doppler <u>downshifted</u> branch (see Eq. 3). However, we have not made a detailed study of this spectral feature.

In order to determine the growth rate of the wave, the output intensity is measured as a function of the length of the interaction region. This is accomplished by means of an axially movable horse-shoe "kicker" magnet that deflects the electron beam into the waveguide wall at any desired position z, thereby terminating the interaction at that point. Fig. 3a shows how the RF power output (within a fixed frequency band of 35 ± 1 GHz) measured at the far downstream end varies with the "kicker" magnet position z. The slope of the curve yields a single pass gain of 0.9 dB/cm. In Fig. 4 the predicted linear growth rate Γ and the efficiency at saturation are plotted as a function of the relative parallel energy spread. The results were obtained from a two-dimensional, self-consistent CARM amplifier code [5]. Comparison of the experimentally measured growth rate with theory implies a beam energy spread in the CARM region $\Delta\gamma_{\parallel}/\gamma_{\parallel} \simeq 0.1$. This is approximately

an order of magnitude worse than the energy spread leaving the emittance selector. In the superradiant mode the amplifier does not reach saturation, so that the observed RF output power is low ($\sim$ 100 kW). In the amplifier mode of operation, we have injected 30 kW of RF power from a 35 GHz magnetron into the launcher illustrated in Fig. 1b. The output power as a function of interaction length is shown in Fig. 3b. The saturated power output is 10 MW, corresponding to an electronic efficiency of 3.3%.

In conclusion, we have reported on the operating characteristics of a CARM amplifier. It appears that emittance growth in the wiggler region prevents the attainment of significantly higher RF power output. We note that the Doppler downshifted mode can become absolutely unstable [9] and thereby cause serious deterioration of the CARM amplifier. However, calculations show [9] that this is of no concern in our parameter regime, since we operate well below the critical current (4.2 kA) and the critical magnetic field ($B_{\parallel} =$ 11.4 kG) for onset of the absolute instability.
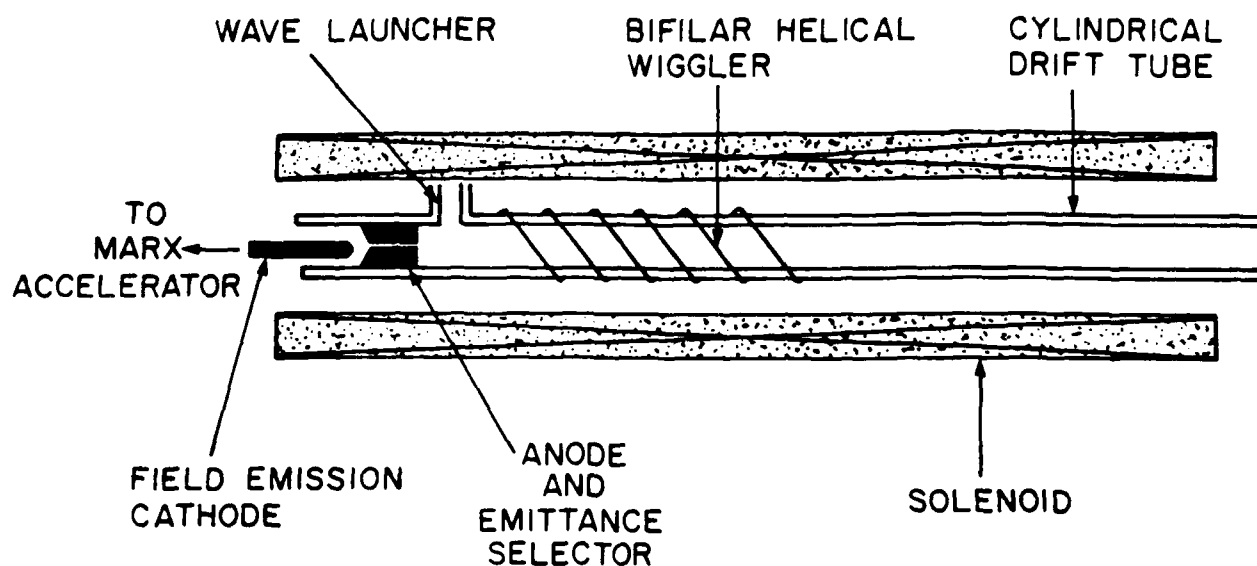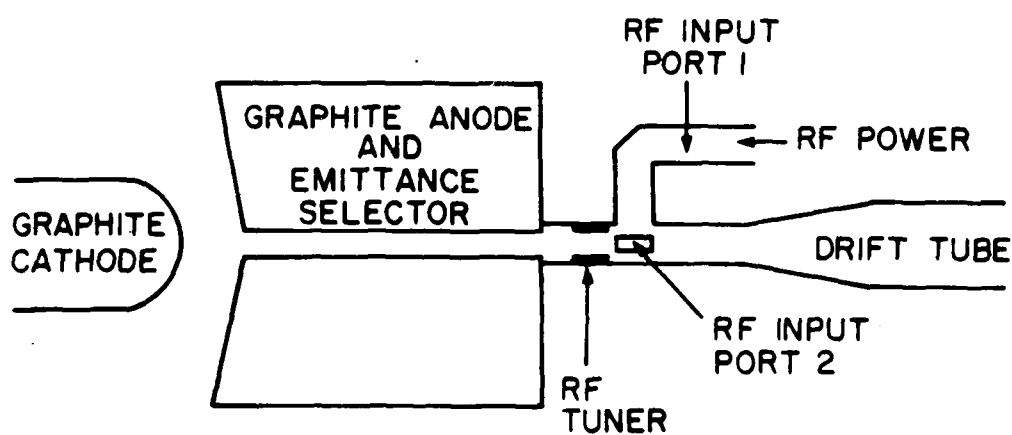
References

[1] A.W. Fliflet, Int. J. Electron., **61**, 1049-1080 (1986).

[2] V.L. Bratman, N.S. Ginzburg, G.S. Nusinovich, M.I. Petelin and P.S. Strelkov, Int. J. Electron., **51**, 541-567 (1981).

[3] K.D. Pendergast, B.G. Danly, R.J. Temkin, and J.S. Wurtele, to be published in IEEE Trans. Plasma Sci.

[4] A.T. Lin, Int. J. Electron., **57**, 1097-1108 (1984).

[5] B.G.Danly, K.D. Pendergast, R.J. Temkin, and J.A. Davies, Proc. SPIE **873**, (1988).

[6] I.E.Botvinnik, V.L.Bratman, A.B.Volkov, N.S.Ginzburg, C.G.Denisov, B.D.Kol'chugin, M.M.Ofitserov, and M.I.Petelin, Pis'ma Zh. Eksp. Teor. Fiz., **35**, 418-420 (1982).

[7] I.E. Botvinnik, V.L. Bratman, A.B. Volkov, G.G. Denisov, B.D. Kol'chugin, and M.M. Ofitserov, Pis'ma Zh. Eksp. Teor. Fiz., **8**, 1376-1378 (1982).

[8] The technique is described by D. Prosnitz and E.T. Scharlemann, Lawrence Livemore National Laboratory, ATA Note No. 229, Feb. 22 (1984).

[9] J. A. Davies, MIT Plasma Fusion Report No. JA-88-29 (1988).

Figure Captions

Fig. 1   Schematic of the CARM amplifier experiment.

Fig. 2   Oscilloscope traces of the electron beam voltage, current and the
            radiation intensity. The latter is measured in the superradiant mode of
            operation.

Fig. 3   Radiation intensity at a frequency of 35 GHz, as a function of the
            CARM interaction length; (a) superradiant operation; (b) amplifier operation.

Fig. 4   Computed saturation efficiency and linear growth rate as a function
            of the electron beam energy spread.

WAVE LAUNCHER   BIFILAR HELICAL WIGGLER   CYLINDRICAL DRIFT TUBE

TO MARX ACCELERATOR

FIELD EMISSION CATHODE

ANODE AND EMITTANCE SELECTOR

SOLENOID

(a)

GRAPHITE ANODE AND EMITTANCE SELECTOR

GRAPHITE CATHODE

RF INPUT PORT I

RF POWER

DRIFT TUBE

RF INPUT PORT 2

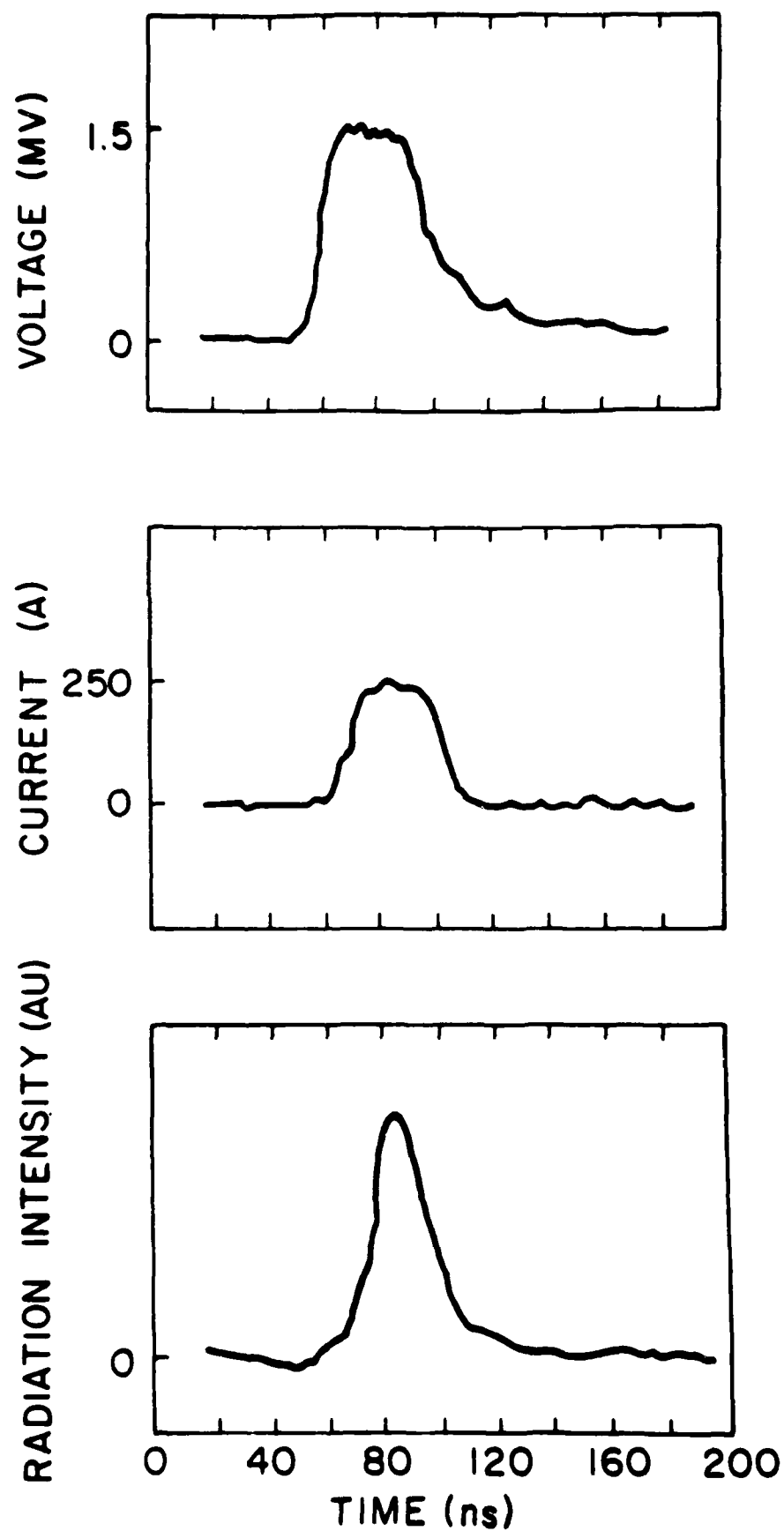RF TUNER

(b)

Fig.1. Bekefi, DiRienzo
Leibovitch,Danly
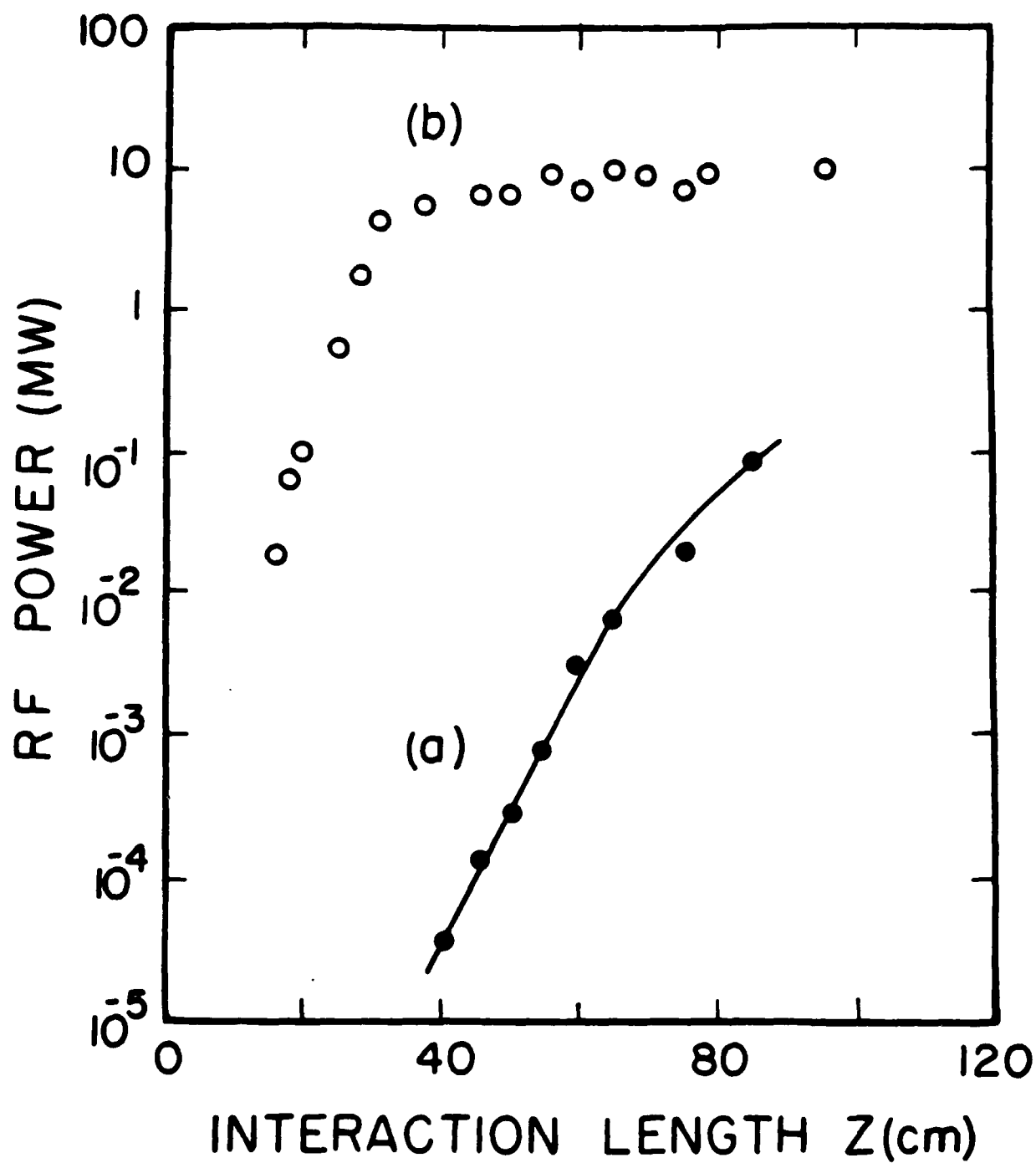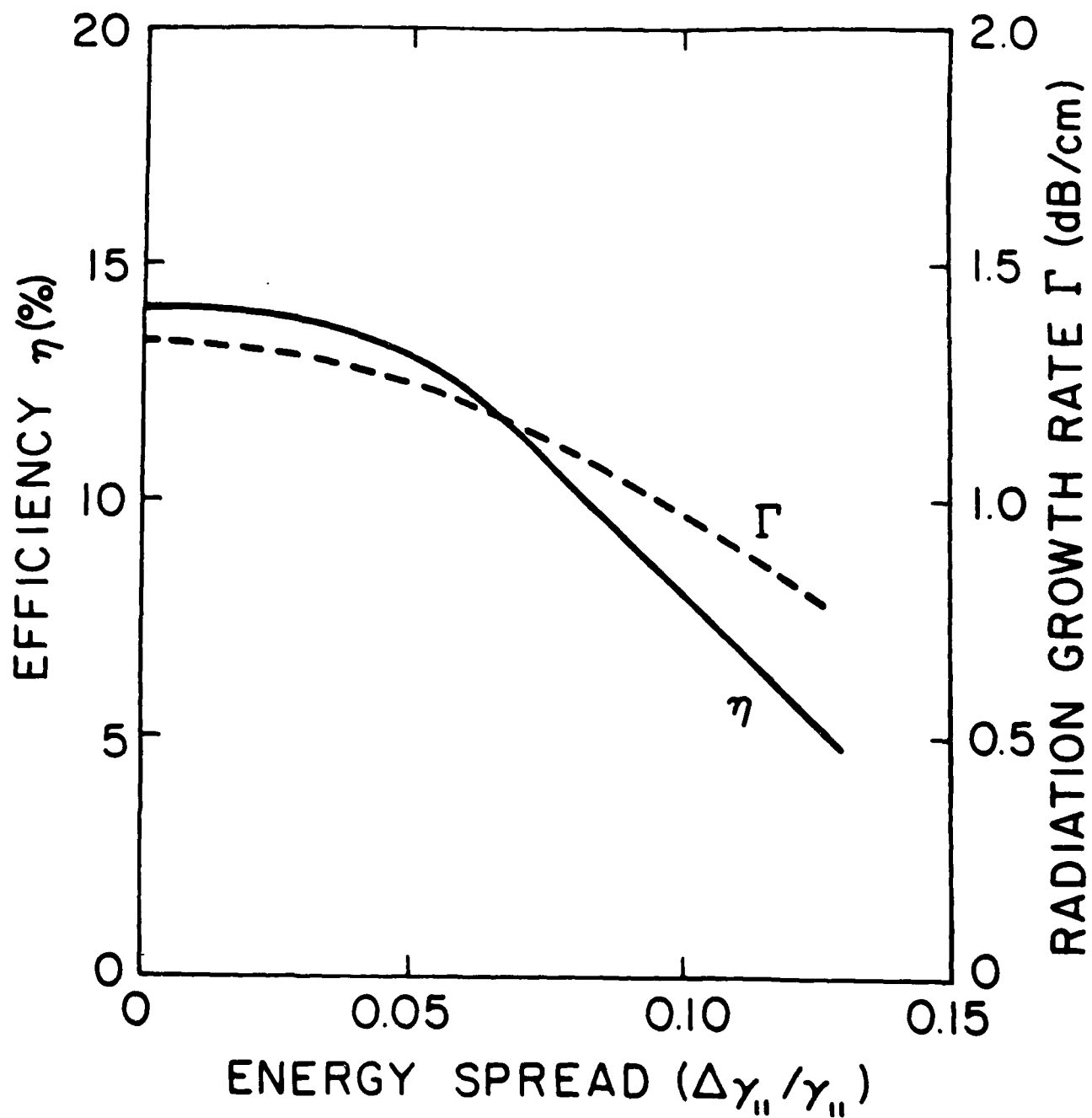
Fig.2. Bekefi,DiRienzo,
Leibovitch,Danly

Fig.3 Bekefi,DiRienzo,Leibovitcl
        Danly

Fig.4. Bekefi,DiRienzo
Laibovitch,Danly